Force Generation and Phosphate Release Steps in Skinned Rabbit Soleus Slow-Twitch Muscle Fibers

Gang Wang and Masataka Kawai
Department of Anatomy and Cell Biology, College of Medicine, The University of Iowa, Iowa City, Iowa 52242 USA

ABSTRACT The force-generation and phosphate-release steps of the cross-bridge cycle in rabbit soleus slow-twitch muscle fibers (STF) were investigated using sinusoidal analysis, and the results were compared with those of rabbit psoas fast-twitch fibers (FTF). Single fiber preparations were activated at pCa 4.40 and ionic strength 180 mM at 20°C. The effects of inorganic phosphate (Pi) concentrations on three exponential processes, **B**, **C**, and **D**, were studied. Results are consistent with the following cross-bridge scheme:

$$\text{AMDP} \underset{k_{-4}}{\overset{k_4}{\rightleftharpoons}} \text{AM*DP} \overset{K_5}{\longleftrightarrow} \text{AM*D} + \text{P}$$

(Step 4 / Step 5)

where A is actin, M is myosin, D is MgADP, and P is inorganic phosphate. The values determined are $k_4 = 5.7 \pm 0.5\ s^{-1}$ (rate constant of isomerization step, $N = 9$, mean ± SE), $k_{-4} = 4.5 \pm 0.5\ s^{-1}$ (rate constant of reverse isomerization), $K_4 = 1.37 \pm 0.13$ (equilibrium constant of the isomerization), and $K_5 = 0.18 \pm 0.01\ mM^{-1}$ (Pi association constant). The isomerization step (k_4) in soleus STF is 20 times slower, and its reversal (k_{-4}) is 20 times slower than psoas fibers. Consequently, the equilibrium constant of the isomerization step (K_4) is the same in these two types of fibers. The Pi association constant (K_5) is slightly higher in STF than in FTF, indicating that Pi binds to cross-bridges slightly more tightly in STF than FTF. By correlating the cross-bridge distribution with isometric tension, it was confirmed that force is generated during the isomerization (step 4) of the AMDP state and before Pi release in soleus STF.

INTRODUCTION

Muscle utilizes the chemical energy of ATP hydrolysis to generate force. The study of the isolated actomyosin system has shown that about half of the free energy change of hydrolysis accompanies the inorganic phosphate (Pi) release step (White and Taylor, 1976). This observation led to the hypothesis that the Pi-release step corresponds to the force-generation step. More recent studies on rabbit psoas fibers demonstrated that the Pi release takes place in two steps, first the isomerization of the weakly attached state to the strongly attached state, and this is followed by the actual Pi release (Kawai and Halvorson, 1991; Fortune et al., 1991; Dantzig et al., 1992; see also Walker et al., 1992). These reports also demonstrated that force generation occurs with isomerization, and the same force is maintained with the Pi release. In contrast, very little is known about slow-twitch skeletal muscle fibers (STF). Millar and Homsher (1992) studied rabbit soleus fibers using caged Pi. However, their finding that force is generated before Pi release was inconclusive, because the concentration of Pi liberated by photolysis of caged Pi was limited to 2 mM, hence their results can be interpreted either in the one-step mechanism or in the two-step mechanism.

As in fast-twitch fibers (FTF), Pi depresses the isometric tension in STF (Altringham and Johnston, 1985; Nosek et al., 1987, 1990; Millar and Homsher, 1992; Stienen et al., 1992; Fryer et al., 1995; Potma et al., 1995). The extent of this inhibition appears to vary among different fiber types and among different studies. These variations led to speculation that the affinity of Pi to cross-bridges may be different among different fiber types.

The steps involved in force generation can be investigated by studying the effect of Pi on the apparent rate constants by using sinusoidal analysis. With this method, the Pi concentration can be tested in the range 0 mM and 30 mM (or higher), and the rate constant ranging from 0.5 to 2000 s^{-1} can be probed. In this report, we provide evidence that in soleus STF, Pi is released by the two-step mechanism similar to psoas FTF. We demonstrate that force is generated with the isomerization of the actin-myosin-ADP-Pi state, and the same force is maintained after the Pi release. The isomerization step is ~20× slower than that of FTF. We also demonstrate that Pi binds to cross-bridges with slightly higher affinity in rabbit soleus STF than rabbit

Received for publication 22 July 1996 and in final form 17 April 1997.

Address reprint requests to Dr. Masataka Kawai, Department of Anatomy and Cell Biology, University of Iowa, Bowen Science Building, 1-670, Iowa City, IA 52242. Tel.: 1-319-335-8101; Fax: 1-319-335-7198; E-mail: masataka-kawai@uiowa.edu.

0006-3495/97/08/878/17 $2.00

psoas (FTF). Preliminary accounts of the present results were presented in Biophysical Society meetings (Wang et al., 1994; Wang and Kawai, 1995).

METHODS

Muscle preparations and experimental solutions

Single fibers were prepared from rabbit soleus muscles as described in Wang and Kawai (1996). The fibers were classified as FTF and STF based on the frequency profile of the results of sinusoidal analysis in the control-activating solution, and only those exhibiting an STF response were used for the present report. This selection procedure was described earlier (Wang and Kawai, 1996).

The relaxing solution (R) contained (in mM): 5.03 EGTA, 0.97 CaEGTA (pCa 7.0), 2 MgATP, 5 ATP, 55 KProp, 61 NaProp, 10 MOPS, 10 NaN_3, and 80 units/ml CK. The control-activating solution (A) contained: 6 CaEGTA, 0.174 $CaProp_2$, 5.76 MgATP, 1.36 ATP, 15 CP, 8 $K_{1.5}Pi$, 53 KProp, 1 NaProp, 10 MOPS, 10 NaN_3, and 80 units/ml CK. A new rigor solution denoted as Rg3 contained: 1 $MgProp_2$, 8 $K_{1.5}Pi$, 100 KProp, 76 NaProp, 10 MOPS, and 17.6 units/ml apyrase (Grade VII, Sigma Chemical Co.). WP solution contained (in mM): 5.82 MgATP, 1.17 free ATP, 15 CP, 90 KProp, 1 NaProp, 10 MOPS, and 80 units/ml creatine kinase (CK). The WP solution was used to remove EGTA and Pi before Ca^{2+} activation. The 0P solution contained 6 CaEGTA, 0.176 $CaProp_2$, 5.80 MgATP, 1.36 ATP, 15 CP, 71.6 KProp, 1 NaProp, 10 MOPS, 10 NaN_3, and 80 units/ml CK. The 30P solution contained 6 CaEGTA, 0.168 $CaProp_2$, 5.67 MgATP, 1.36 ATP, 30 $K_{1.5}Pi$, 15 CP, 1.9 KProp, 1 NaProp, 10 MOPS, 10 NaN_3, and 80 units/ml CK. The solutions with intermediate Pi concentration (2P, 4P, 8P, 16P) were made as appropriate mixtures of 0P and 30P solutions. The 8P solution is the same as the control activating solution (A). In all solutions used for experiments, the ionic strength was adjusted to 180 mM with Na/K propionate (close to that in living muscle cells: Godt and Maughan, 1988), except for the relaxing and rigor solutions that had ionic strength of 200 mM. In all solutions, pH was adjusted to 7.00 ± 0.01. EGTA, CaEGTA, and Pi were added as neutral K salts; MgATP, CP, and free ATP were added as Na_2MgATP, Na_2CP, and $Na_2K_{1.7}ATP$, respectively (all are neutral salts). Individual concentrations of multivalent ionic species were calculated using our computer program, ME, which assumed multiple equilibria with the following apparent association constants (log values at pH 7.00): CaEGTA 6.28, MgEGTA 1.61, CaATP 3.70, MgATP 4.00, CaCP 1.15, and MgCP 1.30. The calculated pCa of all activating solutions was 4.40, and $[Mg^{2+}]$ was 0.5 mM. The temperature was controlled to 20.0 ± 0.2°C in all experiments in this report, and the solution in which the muscle fiber was bathed was continuously stirred to minimize possible local heterogeneities in concentration and temperature.

Experimental procedure

Our earlier work includes a detailed description of the methods used for obtaining complex modulus data and extracting the apparent rate constants of exponential processes (Kawai and Brandt, 1980). In brief, a single skinned muscle fiber was bathed in the relaxing solution and its length L_0 was adjusted so that the sarcomere length of 2.5 μm was achieved by He-Ne laser diffraction. In the relaxing solution a baseline record of the complex modulus was first collected. The preparation was rinsed twice with the WP solution, which contained the same ingredients as the activating solution, except for Ca^{2+}, EGTA, or Pi. The solution was then replaced twice with an activating solution (solution A, 0P, 2P, 4P, 8P, 16P, or 30P) that contained Ca^{2+} (pCa 4.40). When isometric tension fully developed, the length of the fiber was changed in sine waves with 19 different frequencies (0.07–100 Hz corresponding to 1.5–2300 ms in time domain), and the concomitant tension time courses were collected. Thereafter, the preparation was relaxed with two full-volume changes of relaxing solution. The amplitude of the length change was 0.125% ± 0.002% L_0 in all frequencies. This amplitude corresponded to 1.6 nm per half sarcomere.

The complex modulus Y(f) is defined as the ratio of the stress change to the strain change in the frequency (f) domain and represented by a vector in the Nyquist plot. The dynamic modulus is defined as the length of the Y(f) vector, and the phase shift is defined as the angle from the abscissa of the Y(f) vector. The real part of the complex modulus is called the elastic modulus and the imaginary part the viscous modulus. In the beginning and at the end of experiments, the preparation was activated with the control-activating solution, and only those preparations with >80% tension reproducibility were further analyzed. For fibers that developed ≥80% control tension after several activations, the sarcomere length remained at 2.5 μm when detected by laser diffraction. All the modulus data were corrected against those from rigor by the method as developed in Appendix 1 of Kawai and Brandt (1980), except for those shown in Fig. 7, which were corrected against fixed fibers with 2% glutaraldehyde.

RESULTS

Effect of Pi on the complex modulus Y(f) and the apparent rate constants

Rabbit soleus STF (single fibers) were activated with a series of Pi solutions and the complex modulus data Y(f) were collected at 19 discrete frequencies (f). Fig. 1 shows the result plotted in the dynamic modulus versus frequency (*A*), in the phase shift versus frequency (*B*), and in the Nyquist plot (*C*) at four different Pi concentrations. As seen in Fig. 1 *A*, an increase in the Pi concentration shifts the dynamic modulus versus frequency plot to the right. In Fig. 1 *B*, it is seen that an increase in the Pi concentration similarly shifts the phase versus frequency plot to the right. These results imply that cross-bridge kinetics became faster at higher Pi concentrations. Fig. 1 *C* shows the Nyquist plot of the same data, i.e., the plot of the viscous modulus versus elastic modulus. The viscous modulus is the 90° out-of-phase (quadrature) component of Y(f), and the elastic modulus is the in-phase component of Y(f). The Nyquist plots reveal three hemicircles. Because one hemicircle represents one exponential process (Kawai and Brandt, 1980), we infer that Y(f) can be resolved into three exponential processes: **A**, **B**, and **C**, defined in the order of increasing speed. Since there is a mismatch between the data and the equation at the high-frequency end, an extra exponential process, **D**, is added:

$$Y(f) = H + \underbrace{A/(1 + a/fi)}_{\text{Process A}} - \underbrace{B/(1 + b/fi)}_{\text{Process B}} + \underbrace{C/(1 + c/fi)}_{\text{Process C}} + \underbrace{D/(1 + d/fi)}_{\text{Process D}} \quad (1)$$

where $i = \sqrt{-1}$. Of these, three exponential processes are indicated in Fig. 1 *C* by **B**, **C**, and **D**. Process **A** is not well defined in STF. Lowercase letters ($a < b < c < d$) represent characteristic frequencies of exponential processes, and uppercase letters (A, B, C, D) represent their respective magnitudes; 2π times the characteristic frequencies are the apparent (measured) rate constants. H is the elastic modulus extrapolated to zero (0) frequency. The elastic modulus extrapolated to the infinite (∞) frequency is defined as:

$$Y_\infty = H + A - B + C + D \quad (2)$$

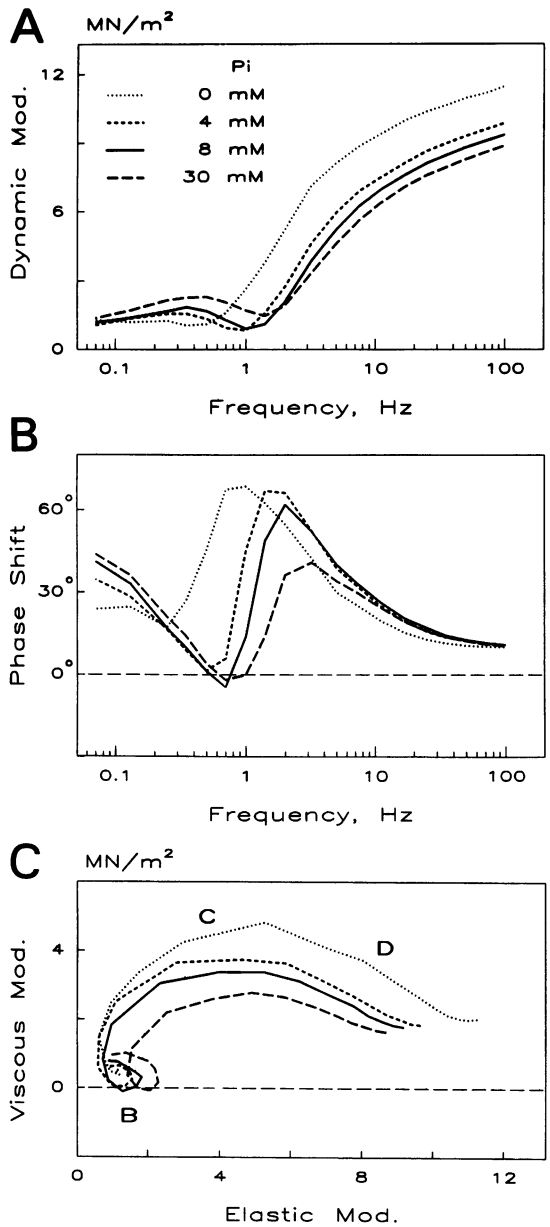

FIGURE 1 The effect of Pi (0 mM, 4 mM, 8mM, and 30 mM) on the complex modulus Y(f) of rabbit soleus STF is plotted in dynamic modulus [= |Y(f)|] versus frequency (*A*), in phase shift [= Arg Y(f)] versus frequency (*B*), and in viscous modulus [= Imag Y(f)] versus elastic modulus [= Real Y(f)] (*C*) (Nyquist plot). The $MgATP^{2-}$ concentration was fixed to 5 mM. Average of nine experiments. The frequencies used are 0.07, 0.13, 0.25, 0.35, 0.5, 0.7, 1.0, 1.4, 2.0, 3.2, 5.0, 7.5, 11, 17, 25, 35, 50, 70, and 100 Hz. In the Nyquist plot (*C*), the low frequency end is near the origin, and the high frequency end is to the right of the plot. Exponential processes **B**, **C**, and **D** are indicated in *C*. The data were corrected against rigor. Unit of phase shift is degree, and that of modulus is $10^6 N/m^2$.

where Y_∞ corresponds to phase 1 of step analysis (Huxley and Simmons, 1971; Heinl et al., 1974; Kawai and Brandt, 1980), and is also referred to as "stiffness" in this report. Process **D** corresponds to the fast component of phase 2, process **C** to the slow component of phase 2 (Ford et al., 1977), and process **B** to phase 3 of step analysis. Process **B** is also known as the "oscillatory work" component (Machin and Pringle, 1960; Rüegg et al., 1971; Kawai and Brandt, 1980) in sinusoidal analysis, or "delayed tension" (Machin and Pringle, 1960; Mannherz, 1970; Herzig et al., 1982) in step analysis. Process **A** corresponds to phase 4 of step analysis.

Fig. 1 *A* illustrates that the dynamic modulus assumes minimal value at ~0.5–1.4 Hz, and this frequency approximates characteristic frequency b. Fig. 1 *B* demonstrates that the phase shift assumes maximal value at 1–3 Hz, and this frequency approximates characteristic frequency c. The fiber generates oscillatory work at the characteristic frequency b and absorbs work at the characteristic frequency c. As seen in Fig. 1, both minimal and maximal frequencies increased with an increase in the Pi concentration. Although the presence of process **B** is evident in the Nyquist plot (Fig. 1 *C*) as represented by the negatively projecting hemicircle, much of the oscillatory work generated is absorbed by neighboring processes **A** and **C**, hence the net result is mostly positive viscous modulus (positive phase shift), as represented in Fig. 1, *B* and *C*.

The complex modulus data were fitted to Eq. 1, and the apparent rate constants ($2\pi a$, $2\pi b$, $2\pi c$, $2\pi d$) were extracted. The apparent rate constants ($2\pi b$, $2\pi c$, $2\pi d$) were averaged for nine experiments and plotted in a logarithmic scale against the Pi concentration in Fig. 2 *A*. This figure demonstrates that the apparent rate constants increase with an increase in the Pi concentration; the effect of Pi is the largest on $2\pi b$, and the smallest on $2\pi d$. (The ratio of values at 30 mM Pi to those at no added Pi are 2.50 ± 0.03, 1.74 ± 0.14, and 1.38 ± 0.11, for $2\pi b$, $2\pi c$, and $2\pi d$, respectively; $N = 9$.) The significance of the effect of Pi on $2\pi b$ is similar to that observed on rabbit psoas fibers (Kawai, 1986; Kawai and Halvorson, 1991; Kawai and Zhao, 1993), except that the rate constants are generally an order of magnitude smaller in rabbit soleus STF than in psoas STF. The Pi effect on $2\pi b$ is generally consistent with its effect on the optimal frequency of oscillatory work in insect muscles (White and Thorson, 1972; Marcussen and Kawai, 1990), and with its effect on the time constant of the delayed rise in tension (phase 3) in cardiac muscles (Herzig and Rüegg, 1977). The Pi effect on $2\pi b$ is also consistent with that in ferret myocardium (Kawai et al., 1993). The rate constant $2\pi b$ is the same as the reciprocal of the time constant of phase 3, and characteristic frequency b is similar to the optimal frequency of oscillatory work (Machin and Pringle, 1960). In Fig. 2 *B*, the apparent rate constant $2\pi b$ is plotted in a linear scale against the Pi concentration. As seen in this figure, $2\pi b$ increased when the Pi concentration was raised, and this effect reached saturation when the Pi concentration was raised further.

Confidence limit of fitted parameters

Because there are nine fitting parameters involved in Eq. 1, and the complex modulus data were collected only at 19

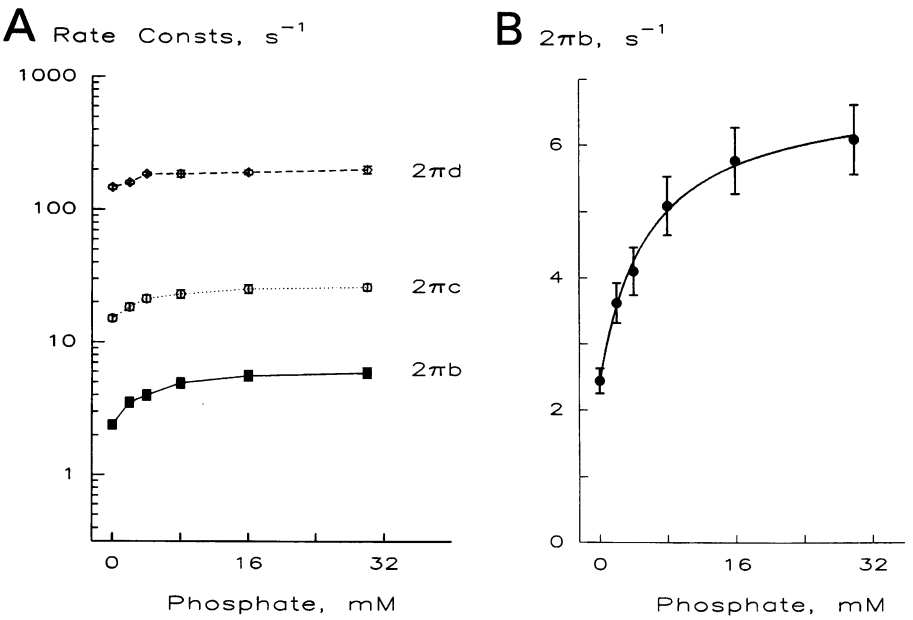

FIGURE 2 (*A*) The apparent rate constants $2\pi b$, $2\pi c$, and $2\pi d$ are plotted in a logarithmic scale against the Pi concentration ($N = 9$, 5 mM $MgATP^{2-}$) for the same experiments shown in Fig. 1. Data points are connected by straight lines. (*B*) The apparent rate constant $2\pi b$ is plotted in linear scale against the Pi concentration ($N = 9$, 5mM $MgATP^{2-}$) for the same data. The curved line is the theoretical projection based on Eq. 4. The data are plotted with mean ± SE error bars. Those smaller than the symbol size cannot be seen.

frequencies, one may consider that the confidence range of each fitted parameter might be large. This is a misconception. Because two quantities (elastic and viscous moduli) are measured at each frequency, the degree of freedom (N_{df}) for a single measurement is 29 ($19 \times 2 - 9$), which is significantly large. Furthermore, because the same experiments were repeated for nine preparations and averaged, N_{df} increases to 333 ($19 \times 2 \times 9 - 9$) when all the data were simultaneously fitted to Eq. 1. This fact results in a narrow range of confidence limit. The 95% confidence limit for the standard condition ([Pi] = 8 mM) was calculated by the method described in Appendix 2 of Kawai and Brandt (1980) for single and multiple measurements, and listed in Table 1. As this table illustrates, taking multiple measurements makes the confidence limit narrower. In addition, a relatively large magnitude of the exponential process results in a narrow confidence limit in the rate constant. It is seen from Table 1 that the rate constant $2\pi b$ can be calculated to be as accurate as −6% to +22%. The confidence limit of $2\pi c$ (−9% to +8%) is smallest because the magnitude C is largest. The confidence limit of $2\pi d$ (−23% to +30%) is larger than that of $2\pi b$ or $2\pi c$. This is because the magnitude D is significantly smaller than magnitude B or C, and process **D** is recognized only as a shoulder in the Nyquist plot (Fig. 1 *C*). Similarly, the confidence limit of $2\pi a$ (−26% to +11%) is larger than that of $2\pi b$, because magnitude A is smaller than magnitude B. In addition, because the lowest frequency of observation is 0.07 Hz, the characterization of process **A** is truncated at this frequency; therefore, $2\pi a$ has a larger negative confidence limit (−26%) than the positive confidence limit (+11%). The confidence limits for other Pi conditions are similar.

Cross-bridge models

There are two ways to explain the Pi effect. These are depicted in Schemes 4 and 5.

TABLE 1 95% Confidence limits of parameters of exponential processes

Parameters	Best fit	95% confidence limits		Units
		Single measurement ($N = 1$)	Multiple measurements ($N = 9$)	
$2\pi a$	1.90	1.20–2.43 (63–128%)	1.41–2.10 (74–111%)	s^{-1}
$2\pi b$	4.11	3.49–5.53 (85–135%)	3.86–5.01 (94–122%)	s^{-1}
$2\pi c$	26.1	22.1–30.5 (84–117%)	23.9–28.2 (91–108%)	s^{-1}
$2\pi d$	202	121–338 (60–167%)	156–262 (77–130%)	s^{-1}
H	0.75	0.53–1.22 (71–163%)	0.67–1.08 (89–144%)	MN/m^2
A	3.90	3.67–4.43 (94–114%)	3.82–4.28 (98–109%)	MN/m^2
B	5.55	5.01–5.81 (90–105%)	5.17–5.64 (93–102%)	MN/m^2
C	7.94	7.60–8.57 (96–108%)	7.81–8.36 (98–105%)	MN/m^2
D	2.34	1.90–3.52 (81–150%)	2.19–3.23 (94–138%)	MN/m^2
N_{df}		29	333	

The 95% confidence limits were calculated based on the method described in Appendix 2 of Kawai and Brandt (1980) for the data shown in Fig. 1 (8 mM Pi condition). The confidence limits are also expressed by the fraction of the best-fit values in parentheses. N_{df} = degree of freedom.

SCHEME 4

Step 4

$$\text{AMDP} \underset{k_{-4}}{\overset{k_4}{\rightleftharpoons}} \text{AM*D} + \text{P}$$

where A is actin, M is myosin, D is MgADP, and P is phosphate. In Scheme 4 the equation that relates the rate constants of elementary steps to the apparent rate constant $2\pi b$ is given in Eq. 3:

$$2\pi b = \sigma k_4 + \text{P}k_{-4} \tag{3}$$

SCHEME 5

Step 4 Step 5

$$\text{AMDP} \underset{k_{-4}}{\overset{k_4}{\rightleftharpoons}} \text{AM*DP} \underset{K_5}{\longleftrightarrow} \text{AM*D} + \text{P}$$

In Scheme 5 the equation that relates the rate and association constants of elementary steps to the apparent rate constant $2\pi b$ is given in Eq. 4 (Kawai and Halvorson, 1991; Zhao and Kawai, 1993).

$$2\pi b = \sigma k_4 + \frac{K_5\text{P}}{1 + K_5\text{P}} k_{-4} \tag{4}$$

where

$$\sigma = \frac{K_2K_{1b}K_{1a}\text{S}}{1 + (1 + K_{1b} + K_{1b}K_2)K_{1a}\text{S}} \tag{5}$$

In these equations, S and P indicate respective ligand concentrations in algebraic expressions: $\text{S} = [\text{MgATP}^{2-}]$ and $\text{P} = [\text{Pi}]_{\text{total}}$. In both schemes, we assume that step 4 is monitored by process **B**. σ is multiplied to k_4 in Eqs. 3 and 4, because there are fast equilibria to the left of Schemes 4 and 5 (not shown here, but shown in Scheme 6 below). $\sigma = 1$ if there is no equilibrium to the left of Schemes 4 and 5.

Scheme 4 is a one-step Pi release and force generation mechanism, in which AMDP represents a weakly attached state (or detached state), and AM*D represents a strongly attached, force-generating state. Scheme 5 is a two-step mechanism, in which an additional AM*DP state is introduced. In this scheme, the AMDP state isomerizes to form the AM*DP state in step 4, and this is followed by the actual release of Pi (step 5). As shown below, the AM*DP state sustains full tension, hence step 4 is the force-generation step.

In the case of Scheme 4, $2\pi b$ is a linear function of P (Eq. 3), whereas in the case of Scheme 5, $2\pi b$ is a hyperbolic function of P (Eq. 4). Thus, the discrimination of these schemes depends on the outcome of the experiments. The results shown in Fig. 2 *B* demonstrate that $2\pi b$ is not a linear function of the Pi concentration, but is a hyperbolic function of the Pi concentration. From this result, we conclude that Scheme 5 explains our results better than Scheme 4.

The data were fitted to Eq. 4, and the kinetic constants were obtained. In Fig. 2 *B*, the curved line is the theoretical projection based on Eq. 4 and best-fit parameters. From this fitting, the following kinetic constants were deduced: $k_4 = 5.7 \pm 0.5\ \text{s}^{-1}$, $k_{-4} = 4.5 \pm 0.5\ \text{s}^{-1}$, and $K_5 = 0.18 \pm 0.01\ \text{mM}^{-1}$ ($N = 9$, mean ± SE); $\sigma = 0.34$ was calculated based on Eq. 5 and the equilibrium constants obtained from the MgATP study (Wang and Kawai, 1996).

TABLE 2 The kinetic constants of elementary steps

Kinetic Constants	Units	Rabbit Soleus STF [Avg ± SE (*n*)]	Rabbit Psoas* [Avg ± SE (*n*)]	Ferret myocardium#	Psoas/Soleus	Myocardium/Soleus
K_0	mM^{-1}	18 ± 4 (7)	2.27 ± 0.05 (7)	ND	0.13	
K_{1a}	mM^{-1}	1.2 ± 0.3 (8)	0.52 ± 0.04 (7)	0.99	0.44	0.8
k_{1b}	s^{-1}	90 ± 20 (8)	2600 ± 400 (7)	270	29	3.0
k_{-1b}	s^{-1}	100 ± 9 (8)	1500 ± 100 (7)	280	15	2.8
K_{1b}	none	1.0 ± 0.2 (8)	1.74 ± 0.20 (7)	0.95	1.7	1.0
k_2	s^{-1}	21 ± 3 (8)	440 ± 30 (7)	48	21	2.3
k_{-2}	s^{-1}	14.1 ± 1.0 (8)	147 ± 6 (7)	14	10	1.0
K_2	none	1.6 ± 0.3 (8)	3.1 ± 0.3 (7)	3.5	2	2.2
σ	none	0.34	0.63	0.61	1.9	1.8
k_4	s^{-1}	5.7 ± 0.5 (9)	121 ± 4 (8)	11	21	1.9
σk_4	s^{-1}	1.92 ± 0.16 (9)	76 ± 3 (8)	6.7	40	3.5
k_{-4}	s^{-1}	4.5 ± 0.5 (9)	89 ± 7 (8)	107	20	24
K_4	none	1.37 ± 0.13 (9)	1.40 ± 0.09 (8)	0.11	1.0	0.08
K_5	mM^{-1}	0.18 ± 0.01 (9)	0.13 ± 0.02 (8)	0.060	0.72	0.3
$k_{-4}K_5$	$\text{mM}^{-1}\text{s}^{-1}$	0.81 ± 0.10 (9)	10.8 ± 1.1 (8)	0.64	13	0.8
k_6	s^{-1}	1.5–3	9–16§	ND	6	

*Results on rabbit psoas were based on the data that used the same experimental solutions as in soleus slow-twitch fibers (STF), except that ionic strength was adjusted to 200 mM, pCa was 4.66, and 160 u/ml CK was used. The kinetic constants of steps 0–2 are from Wang and Kawai (1996).

#Results on ferret myocardium are from Kawai et al. (1993). The data from individual experiments were fitted to respective equations first, and then averaging was performed on the fitted parameters. The fractions are the result of the division of the averaged rabbit psoas value by the averaged rabbit soleus STF, or the division of the averaged ferret myocardium value by the averaged rabbit soleus STF value.

§From Kawai and Halvorson (1991) and Zhao and Kawai (1993). ND, not determined.

For comparative purposes, the Pi study was carried out under similar experimental conditions on rabbit psoas fibers, and the kinetic constants were likewise deduced. These results are summarized in Table 2 together with those from soleus STF.

Combined cross-bridge model

For the purpose of calculating the probability of each cross-bridge state and predicting isometric tension, all the cross-bridge states have to be considered. We have previously developed a cross-bridge scheme surrounding nucleotide binding and cross-bridge detachment steps in soleus STF (Scheme 3 of Wang and Kawai, 1996). In this report we characterized steps surrounding force generation and Pi release (Scheme 5 above). These two schemes can be combined to create the following cross-bridge scheme 6. This scheme has 7 states and is characterized by 7 rate constants and 3 association constants (called "kinetic" constants) that govern transitions between the states.

SCHEME 6

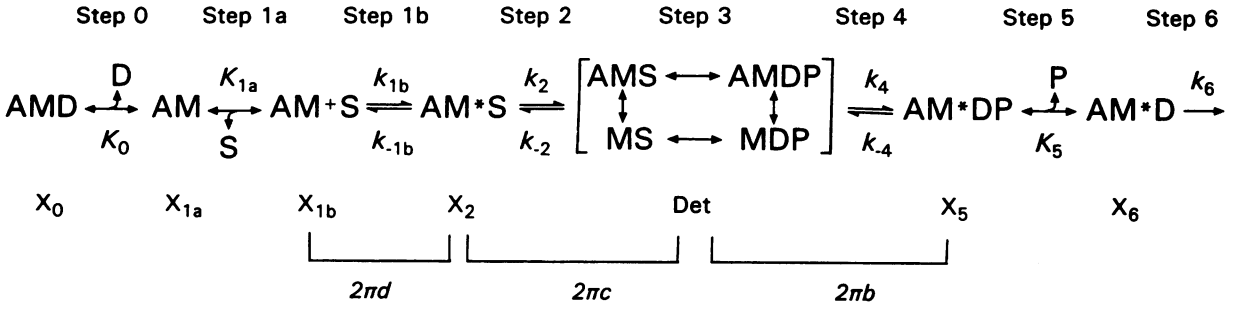

An asterisk (*) or a dagger ($^+$) identifies the second (and the third) conformational state(s). In step 1a, MgATP binds to the rigor-like AM state to form the collision complex AM^+S, which in turn isomerizes in step 1b to form the AM*S state. Cross-bridges then detach in step 2 to form the *Det* state. The *Det* state includes all detached states (MS, MDP) and "weakly attached" states (AMS, AMDP) (Schoenberg, 1988; Brenner et al., 1991). ATP cleavage takes place in step 3 while cross-bridges are detached from actin (MS → MDP) (Bagshaw and Trentham, 1974), or while cross-bridges are weakly attached to actin (AMS → AMDP) (Stein et al., 1979). All detached states (MS, MDP) and weakly attached states (AMS, AMDP) are combined and recognized as the lump-sum detached state (Det) and shown in [ ] in Scheme 6. In step 4, the weakly attached cross-bridges isomerize to form the AM*DP state, which is followed by the release of Pi in step 5 to form the AM*D state. In step 6, AM*D isomerizes to form AMD, which in turn releases MgADP in step 0 to form the AM state. The equation that relates the kinetic constants to the apparent rate constant $2\pi b$ remains the same as Eq. 4, except that σ takes the value between 0 and 1 (Eq. 5).

Probability of cross-bridge states

To predict isometric tension and stiffness as a function of P, S, and D, the probability of each cross-bridge state must be determined. In the following analysis, X_i represents the steady-state probability of cross-bridges in the ith state as shown in Scheme 6. The probability is defined as the fractional concentration of the particular cross-bridge state. The steady-state probability is formulated by assuming the mass action law as an approximation for steps 0–5 (Kawai and Halvorson, 1991; Kawai and Zhao, 1993). Probability is approximately the function of equilibrium constants, and is calculated with Eqs. 6–14 (Zhao and Kawai, 1993).

$$X_0 = K_0 D K_5 P/M \quad \text{(AMD)} \tag{6}$$

$$X_{1a} = K_5 P/M \quad \text{(AM)} \tag{7}$$

$$X_{1b} = K_{1a} S K_5 P/M \quad (AM^+S) \tag{8}$$

$$X_2 = K_{1a} S K_{1b} K_5 P/M \quad \text{(AM*S)} \tag{9}$$

$$X_{34} = K_{1a} S K_{1b} K_2 K_5 P/M \quad \text{(Det)} \tag{10}$$

$$X_5 = K_{1a} S K_{1b} K_2 K_4 K_5 P/M \quad \text{(AM*D)} \tag{11}$$

$$X_6 = K_{1a} S K_{1b} K_2 K_4/M \quad \text{(AM*D)} \tag{12}$$

$$X_{att} \equiv X_0 + X_{1a} + X_{1b} + X_2 + X_5 + X_6 = 1 - X_{34} = 1 - K_{1a} S K_{1b} K_2 K_5 P/M \tag{13}$$

where

$$M \equiv K_{1a} S K_{1b} K_2 K_4 + K_5 P[1 + K_0 D + K_{1a} S(1 + K_{1b} + K_{1b} K_2 + K_{1b} K_2 K_4)] \tag{14}$$

Equations 6–13 are plotted in Fig. 3 by using the equilibrium constants of soleus STF listed in Table 2. As seen in Fig. 3, probability changes hyperbolically with ligand con-

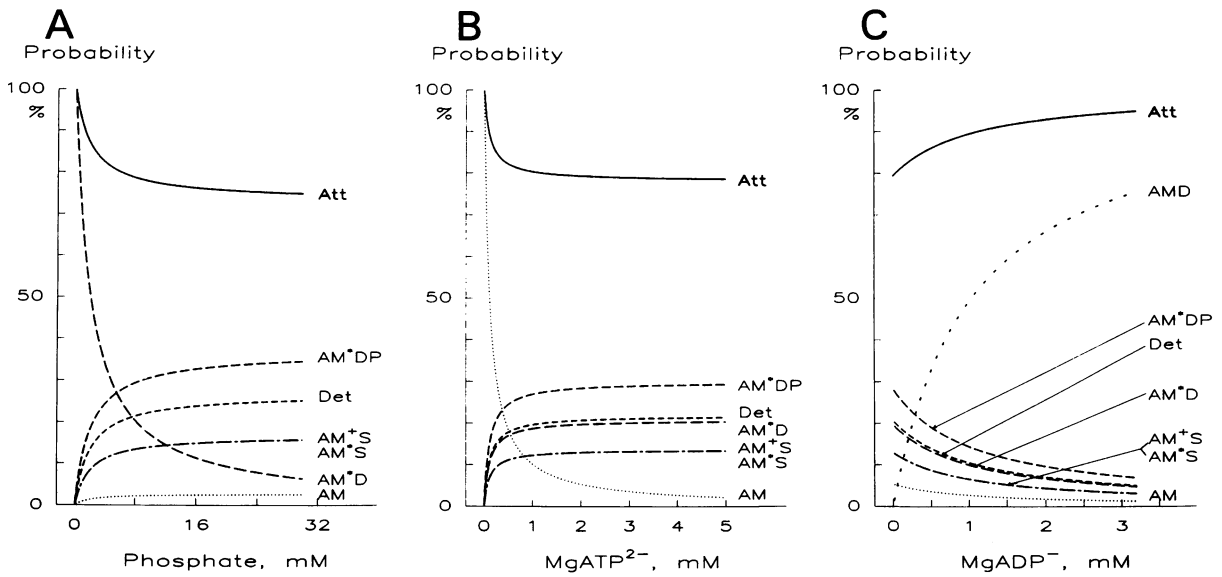

FIGURE 3 Steady-state probabilities of seven cross-bridge states are calculated from Eqs. 6–12 and the averaged equilibrium constants listed in Table 2 for rabbit soleus STF. The probabilities are plotted in percent as functions of total Pi (*A*), $MgATP^{2-}$ (*B*), and $MgADP^{-}$ (*C*) concentrations. For nomenclatures of the cross-bridge states, see Scheme 6. Also included are the summations of the probabilities of (strongly) attached states labeled Att (Eq. 13). The probability of the AMD state is not included in *A* and *B*, because it is small. The parameters of the control conditions (S = 5 mM, D = 0.01 mM, P = 8 mM) are used.

centrations P (phosphate), S (MgATP), and D (MgADP). In Fig. 3, *A* and *B*, the probability of AMD (X_0) is not shown, because it is close to zero (Eq. 6, K_0 = 18 mM^{-1} and D≈0.01 mM in the presence of CP/CK). Because K_{1b} = 1.0 (Table 2), the probability of $AM^{+}S$ and AM*S is the same (Eqs. 8 and 9). Under the control-activating condition (pCa 4.4, P = 8 mM, S = 5 mM, D ≈ 0.01 in the presence of CP/CK) in rabbit soleus STF, the following probabilities are obtained: AMD (0.3%), AM (2.2%), $AM^{+}S$ (13%), AM*S (13%), Det (22%), AM*DP (29%), and AM*D (20%). This can be compared with the probabilities in psoas fibers as 0.2%, 1.6%, 4.2%, 7.4%, 23%, 32%, and 32%, respectively. Therefore, in soleus STF more cross-bridges are populated in the MgATP bound states than in psoas, mainly due to a higher affinity of MgATP to the cross-bridges. Consequently, in soleus STF, fewer cross-bridges are populated in the AM*DP and AM*D states than in psoas. The probability for cross-bridges in the AMD state is small because the estimated MgADP concentration is in the order of 0.01 mM (Meyer et al., 1985) in the presence of CP/CK. The probability of total attached states is 77–78% and does not differ in these two fiber types.

Isometric tension

Isometric tension and stiffness were measured in the same activation as the rate and equilibrium constants. Fig. 4 compares the effect of Pi on isometric tension in soleus STF and with psoas fibers normalized to the tension at 0P (no added Pi). As seen in this figure, Pi depressed tension more in STF than FTF in the low mM range, whereas the degree of suppression did not differ when Pi reached high concentration. The data points in Fig. 5 *A* represent isometric tension plotted against the Pi concentration for the same experiments shown in Fig. 2. As seen in Figs. 4 and 5 *A*, the tension decreased gradually with an increase in the Pi concentration, and the plot was concave upward. The tension versus Pi plot is reminiscent of the probability of all attached cross-bridges (labeled as **Att** in Fig. 3 *A*). The effect of Pi on isometric tension in STF is similar to earlier reports on skeletal (Kawai, 1986; Godt and Nosek, 1989; Stienen et al., 1992; Fryer et al., 1995), insect (Rüegg et al., 1971), and cardiac (Herzig and Rüegg, 1977; Kentish, 1986) muscles.

Although a cross-bridge model can be constructed based on apparent rate constants, actual tension measurement can be used to examine the model's predictability. Assuming that cross-bridges in different states are arranged in parallel in the same half-sarcomere so that their force is additive, isometric tension is modeled as a linear combination (sum) of the probabilities of cross-bridge states (Kawai and Halvorson, 1991; Kawai and Zhao, 1993):

$$\text{Tension} = T_0X_0 + T_{1a}X_{1a} + T_{1b}X_{1b} + T_2X_2 + T_5X_5 + T_6X_6 \quad (15)$$

where X_i (i = 0, 1a, . . . , 6) represents the steady-state probability of the cross-bridges in state i and as defined in Eqs. 6–12, and T_i is its linear coefficient. T_i indicates the value of tension if 100% of the cross-bridges are in state X_i, hence T_i is called the "tension per cross-bridge state." T_{34} is assumed to be 0, because this is the tension from detached or weakly attached cross-bridges.

Eq. 15 is rewritten into Eq. 16, based on the mass action law for step 1b, step 2, and step 4.

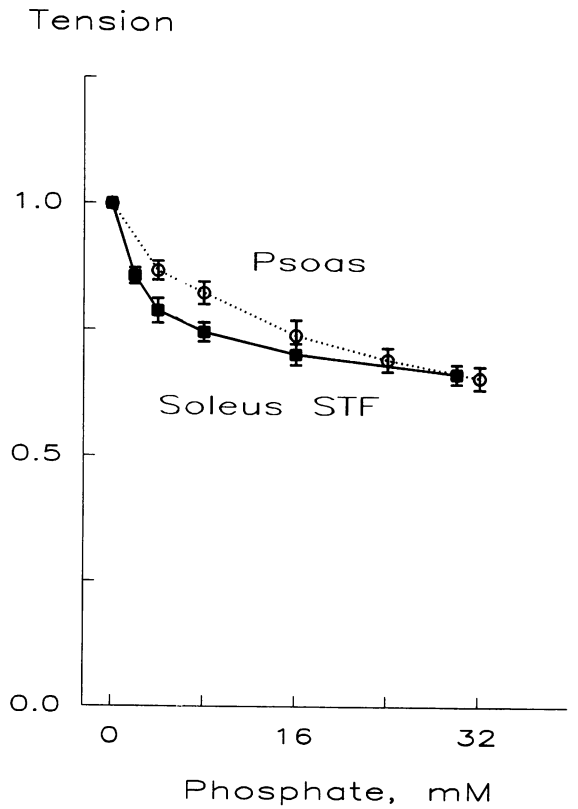

FIGURE 4 Effect of Pi on isometric tension of rabbit soleus STFs and psoas fibers. Isometric tension values at various Pi concentration were normalized to that of 0P solution, averaged, and plotted as a function of the Pi concentration with mean ± SE error bars. (-■-) soleus STF; (····○····) psoas fibers.

$$\text{Tension} = T_0X_0 + T_{1a}X_{1a} + T_xX_{1b} + T_6X_6 \qquad (16)$$

where

$$T_X \equiv T_{1b} + K_{1b}T_2 + K_{1b}K_2K_4T_5 \qquad (17)$$

X_i in Eq. 16 was substituted with analytical forms (Eqs. 6–12), and linear regressions were performed to obtain the coefficients T_i.

When the Pi concentration (P) is increased, AM (X_{1a}) and AM^+S (X_{1b}) increase proportionately, whereas AM*D (X_6) decreases (Fig. 3 *A* and Eqs. 7, 8, and 12). Therefore, if linear fitting is performed on the results of isometric tension as a function of the Pi concentration, the coefficient T_6 and a linear combination of T_{1a} and T_x ($T_{1a} + T_xK_{1a}S$) can be obtained (Eq. 16). In Fig. 5 *A* the curved line represents the best-fit result based on Eq. 16. From this fitting we obtained $T_6 = 1.29\ T_c$. T_i is expressed relative to T_c, that is, the tension in the control activating solution.

Isometric tension as a function of $[MgATP^{2-}]$ and $[MgADP^-]$ is plotted in Fig. 5 *B* and *C*, respectively. These plots are reminiscent of the probability of all attached cross-bridges shown in Fig. 3 *B* and *C*. These data were taken from our previous report (Wang and Kawai, 1996). When the $MgATP^{2-}$ concentration (S) is increased, AM (X_{1a}) decreases, whereas AM^+S (X_{1b}) and AM*D (X_6) increase proportionately (Fig. 3 *B* and Eqs. 7, 8, and 12). Therefore, if linear fitting is performed on the results of isometric tension as a function of the $MgATP^{2-}$ concentration, the coefficient T_{1a} and a linear combination of T_x and T_6 ($T_x + T_6K_{1b}K_2K_4/K_5P$) can be obtained (Eq. 16). Data points in Fig. 5 *B* represent the average isometric tension plotted against the $MgATP^{2-}$ concentration, and the curved line represents the best fit result based on Eq. 16. From this we obtained $T_{1a} = 1.12\ T_c$.

When the $MgADP^-$ concentration (D) is increased, AMD (X_0) increases, whereas AM (X_{1a}), AM^+S (X_{1b}), and X_6 (AM*D) decrease proportionally (Fig. 3 *C* and Eqs. 6–8, 12). Therefore, if linear fitting is performed on the results of isometric tension as the function of the $MgADP^-$ concentration, the coefficient T_0 and a linear combination of T_{1a}, T_x, and T_6 ($T_{1a} + T_xK_{1a}S + T_6K_{1a}SK_{1b}K_2K_4/K_5P$) can be determined (Eq. 16). Data points in Fig. 5 *C* represent the average isometric tension plotted against the $MgADP^-$ concentration, and the curved line represents the best fit result based on Eq. 16. From this we obtained $T_0 = 1.31\ T_c$.

Because X_{1b} (AM^+S), X_2 (AM*S), and X_5 (AM*DP) have the same P, S, and D dependence (Eqs. 8–11; Fig. 3), their coefficients T_{1b}, T_2, and T_5 cannot be determined independently by studies that change Pi, $MgATP^{2-}$, and $MgADP^-$ concentrations (Kawai and Zhao, 1993). However, the Pi and MgATP studies determined T_x that is defined by Eq. 17. Furthermore, since AM^+S is a collision complex, the force in this cross-bridge (T_{1b}) may not be different from the force in the cross-bridge (T_{1a}) before the collision, AM. This is also the case in step 5 (Pi release). Taken together, if we assume $T_{1b} = T_{1a}$ and $T_5 = T_6$, then $T_2 = 0.81\ T_c$ will result. A similar analysis was carried out on the data from rabbit psoas and all T_i values are entered in Table 3 for comparison.

Stiffness (Y_∞)

The stiffness (defined in Eq. 2) for the first approximation is proportional to the probability of strongly attached cross-bridges (X_{att}).

$$Y_\infty = Y_aX_{att} = Y_a(1 - K_{1a}SK_{1b}K_2K_5P/M) \qquad (18)$$

where Y_a is the stiffness of the fiber when all cross-bridges are attached. X_{att} is given in Eq. 13, and M is defined in Eq. 14. The probability of attached cross-bridges is calculated and entered in Fig. 3 (labeled **Att**). Measured Y_∞ is plotted in Fig. 6 as a function of Pi, $MgATP^{2-}$ and $MgADP^-$ concentrations. All stiffness data were normalized to Y_c, which is the stiffness at the control activation. Fig. 6 *A* represents stiffness (Y_∞) plotted against Pi concentration. Y_∞ decreased gradually as the Pi concentration was increased, indicating that fewer cross-bridges were attached at the higher Pi concentration. The stiffness data plotted in Fig. 6 are similar to the probability of attached cross-bridges shown in Fig. 3. The stiffness data from three sets of studies

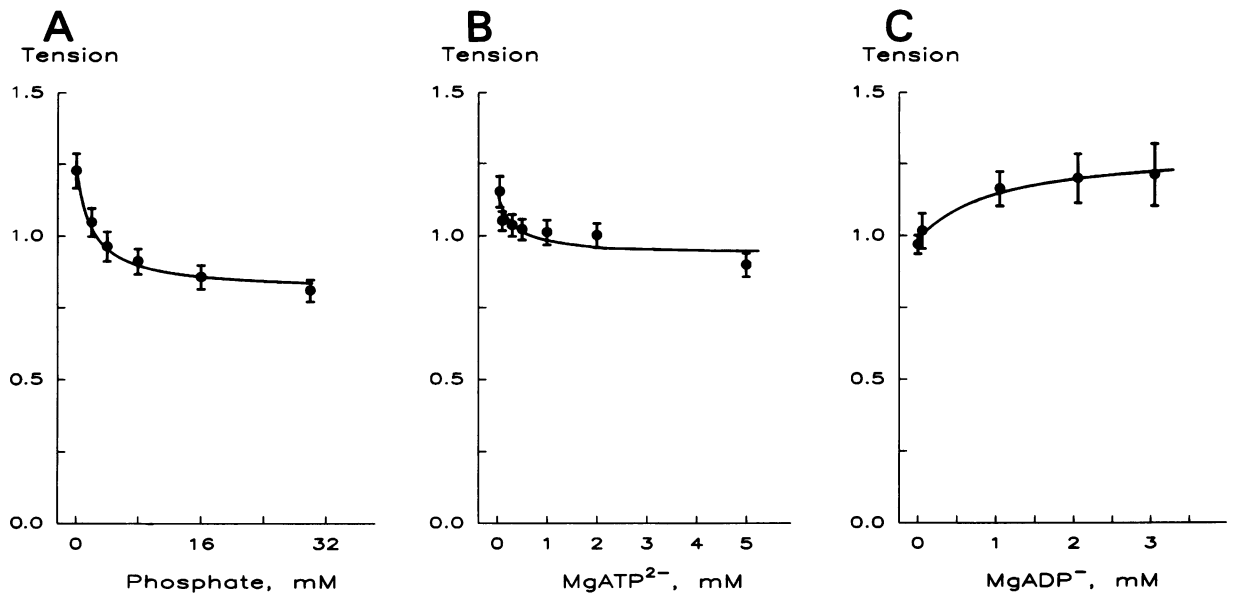

FIGURE 5 (*A*) Isometric tension plotted as a function of the total Pi concentration (N = 9); (*B*) MgATP concentration (N = 8); and (*C*) the MgADP concentration (N = 7). The data were first normalized to the value of initial control tension (T_c, Table 3), then averaged. Theoretical projections (continuous lines) are based on Eq. 16 and the equilibrium constants (Table 2), and the tension/cross-bridge state (Table 3). The averaged values are shown with mean ± SE error bars. The units of all ordinates are T_c.

were fitted to Eq. 18, with theoretical projections based on Eq. 18 denoted by continuous lines. As shown in Fig. 6, fitting was satisfactory in the Pi and ADP studies, and acceptable for the ATP study. From these fittings, Y_a = 98 ± 5 T_c (N = 24) was obtained.

Comparison with the rigor state

To measure the stiffness and tension of the fibers directly when all cross-bridges are attached, the preparation was activated with the control-activating solution, followed by induction of the rigor state by one full volume change with the Rg3 solution that contained 17.6 units/ml apyrase (Fig. 7 *A*). During the control activation T_c was measured, and the complex modulus data Y(f) were collected (Record #10, Fig. 7 *A*). Y(f) was fitted to Eq. 1 to obtain the magnitude A, B, C, D, and H, and Y_∞ (=Y_c) was calculated from Eq. 2. Rigor tension developed in ~0.5 min, and then slowly declined, as seen in Fig. 7 *A*. The rigor tension and the complex modulus Y(f) reached a steady state in 1 min, and they did not change after a further wash with the Rg3 solution. The complex modulus data collected after rigor induction (record #12 in Fig. 7 *A*) were almost independent of frequency (shown in Fig. 7, *B–D*), and similar to those published earlier on rabbit psoas (Kawai and Brandt, 1980). We do not identify any exponential process in the rigor record in the frequency range we studied (Fig. 7 *B*). Thus, we used the modulus at 100 Hz for stiffness of the rigor state (Y_{rig}) that was collected at ~1 min after the rigor induction. Tension and stiffness values were expressed in terms of T_c and averaged. The averaged rigor tension was T_{rig} = 1.08 ± 0.04 T_c (N = 8), which is close to T_{1a} (1.12 ± 0.06 T_c, Table 3) of the AM state. The averaged rigor stiffness was Y_{rig} = 118 ± 7 T_c (N = 8), and it turned out to be not very different from Y_a (=98 ± 5 T_c), the estimated stiffness from active fibers when all cross-bridges are attached. Finally, Y_∞ during control activation was divided by Y_{rig} and averaged. The result was: Y_∞/Y_{rig} = 63 ± 3% (N = 8). This value represents the fraction of attached cross-bridges during the control activation. This fraction turned

TABLE 3 Tension per cross-bridge state

Coefficient	State	Source	Soleus STF [Avg ± SE (n)]	Psoas [Avg ± SE (n)]	Units
T_0	AMD	ADP study	1.31 ± 0.11 (7)	1.34 ± 0.04 (7)	T_c
T_{1a}	AM	ATP study	1.12 ± 0.06 (8)	1.29 ± 0.18 (7)	T_c
T_{1b}	AM$^+$S	Estimate	1.12	1.29	T_c
T_2	AM*S	ATP/Pi studies	0.81	0.89	T_c
T_{34}	Det	Assumption	0	0	T_c
T_5	AM*DP	Estimate	1.29	1.27	T_c
T_6	AM*D	P_i study	1.29 ± 0.05 (9)	1.27 ± 0.06 (8)	T_c
T_c		All studies	142 ± 15 (24)	149 ± 8 (22)	kN/m^2

T_c is tension in the control-activating solution (A).

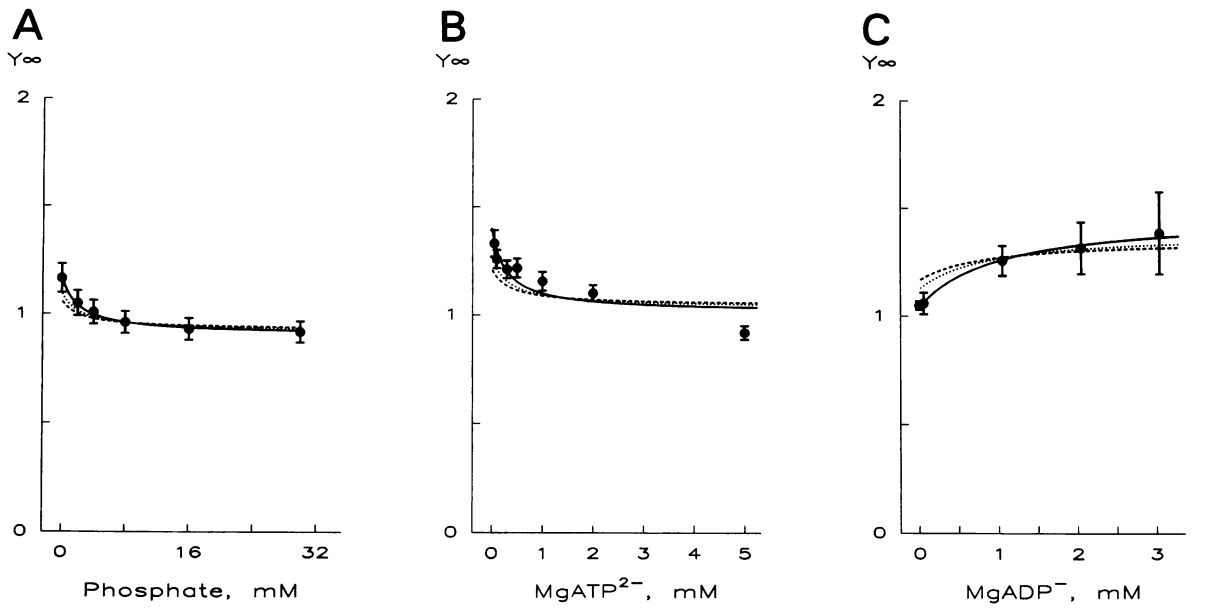

FIGURE 6 Stiffness (Y_∞) plotted as a function of the Pi concentration (N = 9) in (*A*), the MgATP concentration (N = 8) in (*B*), and the MgADP concentration (N = 7) in (*C*). The stiffness data were first normalized to the initial control stiffness (Y_c) of the same preparation, then averaged. The averaged values are shown with mean ± SE error bars. Theoretical projections (*curved lines*) are based on Eq. 20, the equilibrium constants (Table 2), and Y_a. (—), q = 0 (no series compliance); (· · ·), $q = 0.5\ Y_c^{-1} = 0.64\ Y_a^{-1}$ (39% series compliance); (- - -), $q = 1.0\ Y_c^{-1} = 1.27\ Y_a^{-1}$ (56% series compliance).

out to be not far from the expectation (78%), based on the probability calculation of the attached cross-bridges (Eq. 14) during the control activation.

DISCUSSION

In a previous report (Wang and Kawai, 1996), we studied the effect of the MgATP and MgADP concentrations on the apparent rate constants, and deduced the elementary steps surrounding nucleotide binding and cross-bridge detachment (steps 0–2). In this report, we studied the effect of Pi concentration on the apparent rate constants, and deduced the elementary steps surrounding force generation and Pi release steps (steps 4 and 5). These results are combined and summarized in cross-bridge scheme 6 and Table 2. Our findings demonstrate that the cross-bridge scheme of STF from rabbit soleus muscle is not any different from that of rabbit psoas (a FTF) (Zhao and Kawai, 1993) or from ferret myocardium (Kawai et al., 1993). Similar to results found with rabbit psoas, we found that force generation takes place at step 4 (Pi isomerization) and before Pi is released in soleus STF. These steps are discussed in the following sections.

Two-step mechanism of force generation and phosphate release

We studied the effect of Pi on $2\pi b$ (the apparent rate constant of process **B**). If the plot of [Pi] versus the apparent rate constant is linear (Eq. 3), then this result is consistent with the one-step Pi release and force generation mechanism as shown in Scheme 4. If the plot is hyperbolic (Eq. 4), then this result is consistent with the two-step Pi release and force-generation mechanism as shown in Scheme 5. Our experiment demonstrates that the plot is hyperbolic (Fig. 2 *B*), hence this result is consistent with the two-step mechanism. In this mechanism, Pi isomerization occurs at step 4, and Pi release occurs at step 5. Force is generated at step 4, and the same force is maintained at step 5. The two-step mechanism in rabbit psoas fibers was proposed by Kawai and Halvorson (1991) using sinusoidal analysis, Fortune et al. (1991) using rapid pressure-release, and by Dantzig et al. (1992) using photolysis of caged Pi (see also Walker et al., 1992). It is important to note that the hyperbolic plot is also consistent with the hypothesis that the Pi-release step is faster than the speed of observation, which is an implicit assumption for deriving Eq. 4 (Kawai and Halvorson, 1991; Zhao and Kawai, 1993).

If the Pi study is limited to the low concentration range ([Pi] $< 1/K_5$), then Eq. 4 reduces to Eq. 3. The rate constant versus [Pi] plot looks linear, and one cannot discriminate one-step versus two-step mechanisms. This was exactly the case in the report of Millar and Homsher (1992) on rabbit soleus, presumably on STF. Since the amount of Pi released by photolysis of caged Pi was limited to 2 mM and their Pi concentration range studied was limited to 1–3 mM, their plot was linear. Our result shows that $1/K_5$ = 5.6 mM in soleus STF, hence the experiment to demonstrate the two step mechanism should be carried out at least twice this concentration and ideally larger. The concentration range

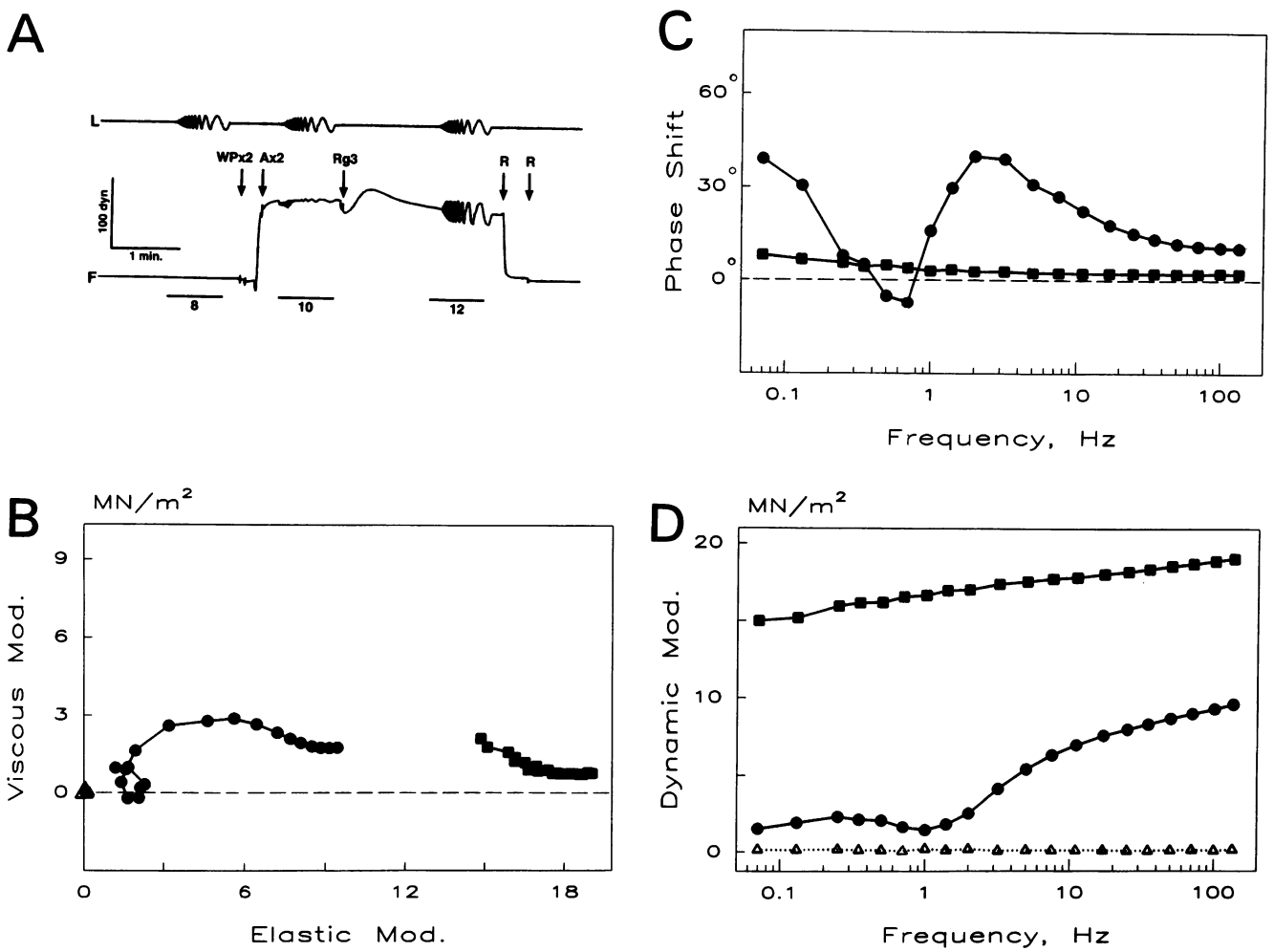

FIGURE 7 (*A*) Slow pen trace of the tension time course of a single STF preparation from rabbit soleus. X2 indicates that the solution was changed twice. The preparation was initially soaked in the relaxing solution (R), which was replaced twice with the washing solution at WP, and replaced twice with the control activating solution at A. The solution was replaced once with the Rg3 solution at Rg3. This solution was replaced twice with the relaxing solution at R. Complex stiffness was collected as seen as oscillations in both length (above) and force (below) traces, and numbered as 8, 10, and 12. Photographically reproduced from the original pen trace. Both length and tension signals were filtered by second-order low pass filters (cutoff frequency: 10 Hz) before traced, hence response at higher frequency is attenuated. The amplitude of length oscillation was kept at 0.125% ± 0.002% L_0 at all frequencies. The frequencies used are 0.07, 0.13, 0.25, 0.35, 0.5, 0.7, 1.0, 1.4, 2.0, 3.2, 5.0, 7.5, 11, 17, 25, 35, 50, 70, 100, and 135 Hz. The data were corrected against those after glutaraldehyde fixation and plotted in (*B*) viscous modulus [= Imag Y(f)] versus elastic modulus [= Real Y(f)] (Nyquist plot) of fiber during relaxation (record #8), activation (record #10), and after rigor formation (record #12); (*C*) phase shift [= Arg Y(f)] versus frequency during activation and rigor; (*D*) Dynamic modulus [= |Y(f)|] versus frequency during relaxation, activation, and rigor. Relaxation: ···△···; Activation: —●—; Rigor: —■—. Unit of the dynamic modulus is MN/m^2 and that of phase shift is degree.

we chose (0–30 mM) is adequate for demonstrating the two step mechanism, because the rate constant vs. [Pi] plot exhibits both an increase and a saturation (Fig. 2 *B*).

The linear plot of Millar and Homsher (1992) can still determine the intercept (σk_4) and the slope ($k_{-4}K_5$) when Scheme 5 is assumed (see Eq. 4). For comparative purposes, we calculated these values in Table 2 (σk_4 = 1.92 s^{-1} and $k_{-4}K_5$ = 0.81 mM^{-1} s^{-1}). They agree with those reported by Millar and Homsher (1992) within a factor of 2.5 (k_{+3} = 1.96 s^{-1} and k_{-3}/K_4 = 1.994 mM^{-1} s^{-1}, respectively, in their nomenclature) at 20°C. Millar and Homsher (1992) did not assume rapid equilibrium to the left of Scheme 5, hence our σk_4 compares to their k_{+3}.

Phosphate contamination

The actual Pi concentration of the Pi study may be somewhat higher than the added concentration of Pi. This is because of the Pi contamination that comes mainly with CP (Millar and Homsher, 1992). Pi is also generated in muscle fibers as a result of ATP hydrolysis. Our previous analysis concluded that the total of 0.62 mM Pi contamination was present in rabbit psoas fibers (Kawai and Halvorson, 1991). Similarly, the total Pi contamination was estimated to be ~0.7 mM by Millar and Homsher (1992). In this case, the Pi axes of all plots should be shifted to the left by the amount of Pi contamination. This shift will change the

kinetic constant slightly, but the change is not large. If we assume the Pi contamination to be 0.6 mM, then k_4 becomes 4.1 instead of 5.7, k_{-4} becomes 5.0 instead of 4.5, and K_5 becomes 0.20 instead of 0.18.

Comparison of elementary steps of soleus STF with psoas and myocardium

From the Pi study, we found k_4 (rate constant of force generating isomerization step) to be 5.7 s^{-1} in rabbit soleus STF, which compares to 121 s^{-1} in psoas (Table 2). Therefore, it can be concluded that the isomerization step (step 4) is 21 times slower in rabbit soleus STF than in psoas under our experimental conditions. This result is consistent with the ~30-fold difference in $2\pi b$ between rabbit psoas FTF and soleus STF (Kawai and Schachat, 1984), and with the time course of the tension transient in response to the step length change (Galler et al., 1994). The rate constant of the reverse attachment step (k_{-4}) is 4.5 s^{-1} in soleus STF, which is 20 times smaller than that in psoas. Consequently, the equilibrium constant of the isomerization step (K_4) is ~1.4 and not any different in these two fiber types, indicating that the free energy change of the isomerization step is not any different between STF and FTF.

The Pi association constant (K_5) is found to be 0.18 ± 0.01 mM^{-1} in rabbit soleus STF, which is slightly higher than the value (0.13 ± 0.02 mM^{-1}) found in psoas (Table 2). The higher affinity of Pi to cross-bridges in soleus can account for the higher Pi sensitivity in suppressing the isometric tension in soleus STF (Fig. 4). This observation is generally consistent with the reports by Altringham and Johnston (1985), Fryer et al. (1995), and Potma et al. (1995). The suppression of Pi on isometric tension at 30 mM Pi in both types of muscle is the same (Fig. 4), which is consistent with the findings of Nosek et al. (1990). However, these observations are at variance with the results of Millar and Homsher (1992) and Stienen et al. (1992), who reported that Pi is less sensitive in suppressing isometric tension in STF (rabbit soleus) than in FTF (rabbit psoas). Although the reason for this discrepancy is not immediately apparent, it may be related to a difference in the experimental conditions. The fact that both equilibrium constants K_4 and K_5 are comparable in STF and FTF (Table 2), respectively, indicates that the basic mechanism of the force-generation step and the Pi-release step is not much different in these two fiber types.

It is interesting to note that the rate constants of the force-generation step (k_4 and k_{-4}) obtained from rabbit soleus STF are smaller than the corresponding rate constants from ferret myocardium (Table 2; Kawai et al., 1993), indicating that the elementary steps in the cross-bridge cycle in soleus STF are slower than in cardiac muscle. The Pi association constant (K_5) of soleus STF is three times larger than that of myocardium. In addition, K_5 of psoas is twice as large as myocardium (Table 2), indicating that myocardium is 2–3 times more resistant against Pi accumulation than skeletal muscles (Kawai et al., 1993).

Reversibility of the Pi-release step in muscle fibers

In solution studies of acto-S1 from fast-twitch muscles, the Pi association constant is found to be 0.1 M^{-1} to 0.01 M^{-1} (Taylor, 1979); hence the Pi release step is practically irreversible, and the large amount of free energy liberated is lost as heat. A large free energy decrease with the Pi release was the basis for suggesting that the Pi-release step may correspond to the force-generation step (White and Taylor, 1976). In solution studies, the force-generating AM*DP state was not recognized, presumably because of the instability of this complex under the unloaded condition. Hence, force generation and Pi release are considered to occur simultaneously, as shown in Scheme 4. In muscle fibers, because the free energy released by ATP-hydrolysis is stored as the potential energy in the elastic portion of the cross-bridges as well as in structures in series with them, the Pi-release step is readily reversible in the presence of the mM concentration of Pi as demonstrated by using isotope ^{32}P (Mannherz, 1970; Rüegg et al., 1971; Ulbrich and Rüegg, 1971; Gillis and Maréchal, 1974) and ^{18}O exchange (Hibberd et al., 1985). Thus, it can be concluded that the total free energy change associated with step 4 is the sum of the free energy change measured by K_4 ($\Delta G^\circ = -RT \ln K_4$) and the potential energy evolution measured by force generation (Kawai and Halvorson, 1991).

Correlation of exponential processes with elementary steps

In a previous study (Wang and Kawai, 1996), we showed that step 1b correlates with process **D**, and that step 2 correlates with process **C**. The present report demonstrates that step 4 correlates with process **B**. These correlations hold true even after Schemes 3 and 5 are combined to result in Scheme 6. For instance, if the correlation of processes **B** and **C** is transposed (if **B** = step 2 and **C** = step 4), it follows that process **C** becomes insensitive to the MgATP concentration, because a slow process **B** interposes between MgATP binding and step 4. This prediction is in apparent contradiction to our results (Fig. 4B of Wang and Kawai, 1996), demonstrating that process **B** could not be correlated with step 2, and that process **C** could not be correlated with step 4. Similarly, the correlation of processes **B** and **D** cannot be transposed.

Because of the model proposed by Huxley and Simmons (1971), it may be considered that fast process **C** or **D** is correlated with the Pi-release step. Process **D** is equivalent to the fast component of phase 2 of step analysis, and process **C** is equivalent to the slow component of phase 2 (Huxley and Simmons, 1971; Ford et al., 1977; Kawai and Brandt, 1980). If process **D** correlates with step 5, it follows that the rate constant of process **D** ($2\pi d$) is insensitive to the MgATP or MgADP concentration, because a slow process **B** intervenes between step 1a (MgATP binding) and step 5. It also follows that $2\pi b$ is linearly related to the Pi concen-

tration. This mechanism apparently contradicts the data shown in Fig. 4A and Fig. 6 of Wang and Kawai (1996), and contradicts the data shown in Fig. 2 *A* of this report. Similarly, process **C** cannot be correlated with step 5, because process **C** is sensitive to the MgATP concentration (Fig. 4B of Wang and Kawai, 1996), and because $2\pi c$ is not linearly related to the Pi concentration (Fig. 2 *A*).

We developed the discussion above assuming that the correlation between processes and elementary steps are perfect. This assumption is only true if $2\pi d \gg 2\pi c \gg 2\pi b$ (Hammes, 1968). In practice, b, c, and d are separated by the factor of 4–10 (Fig. 2 *A*); therefore, there are some cross-correlations between the processes and the steps. The small Pi effect on $2\pi c$ and $2\pi d$ (1.74 and 1.38, respectively, comparing 30P and 0P conditions) and as shown in Fig. 2 *A* is expected based on Scheme 6. This is the very reason why we are focusing on the large effects (such as Pi affects $2\pi b$ most, Fig. 2 *A*) as the first approximation.

Force per cross-bridge state

The effect of Pi on isometric tension in STF (Figs. 4 and 5 *A*) is consistent with earlier reports on skeletal (Rüegg et al., 1971, Altringham and Johnston, 1985; Kawai, 1986; Godt and Nosek, 1989; Nosek et al., 1987, 1990; Pate and Cooke, 1989; Millar and Homsher, 1990, 1992; Kawai and Halvorson, 1991; Stienen et al., 1992; Kawai and Zhao, 1993; Fryer et al., 1995; Potma et al., 1995), insect (Mannherz, 1970; Rüegg et al., 1971; Marcussen and Kawai, 1990), and cardiac (Herzig and Rüegg, 1977; Kentish, 1986, 1991; Godt and Nosek, 1989; Nosek et al., 1990; Kawai et al., 1993) muscles. In both STF and FTF, our results are consistent with the assumption that the cross-bridge force is the same in the AM*DP and AM*D states. Our results demonstrate that force generation occurs at step 4 and with the isomerization of the AMDP state (weakly attached state) to the AM*DP state, but force does not change with the release of Pi (step 5) or subsequent isomerization of the ADP state (step 6). Previous studies with rabbit psoas had the same results using the techniques of sinusoidal analysis (Kawai and Halvorson, 1991; Kawai and Zhao, 1993), pressure-release (Fortune et al., 1991), and caged Pi (Dantzig et al., 1992; see also Walker et al., 1992).

From the results shown in Table 3, it can be further seen that a similar force is maintained in the AMD and AM states. Our results are consistent with the idea that the same force is also maintained in AM and AM^+S states because the AM^+S state is a collision complex. Force then drops with the occurrence of ATP isomerization (step 1b) and disappears at the cross-bridge detachment (step 2). This gradual decline of force is consistent with the fact that both process **D** (step 1b) and process **C** (step 2) are observed as exponential advances (positive terms in Eq. 1).

In both STF and FTF, our analysis implies that the force per cross-bridge state is the largest in the AM*DP and AM*D states (Table 3). This fact implies that force generation occurs only at a single step in the cross-bridge cycle, and force does not increase in gradual steps. However, a gradual increase of force may be seen if the cross-bridge cycle were reversed in step 2 and step 1b (see Table 3).

Rate-limiting step

The cross-bridge cycle is completed (closed) by assuming a slow step 6 between the AM*D and AMD states and as shown in Scheme 6. The AMD state may not be on the cyclic pathway, but the result is the same if we assume that step 6 results directly in the AM state. Step 6 must be slower than any other steps in the cycle, or else the effect of Pi (Fig. 2 *B*), MgATP, and MgADP (Wang and Kawai, 1996) on the apparent rate constants cannot be explained. In a solution study of purified proteins from fast-twitch muscles, two energetically different acto-S1·ADP states were identified (Sleep and Hutton, 1980), which presumably correspond to the AM*D and AMD states of this report.

Since step 6 is the rate-limiting step and limits the ATP hydrolysis rate, the rate constant of this step can be characterized by the ATP hydrolysis rate measurement.

$$\text{ATPase} = k_6[\text{AM*D}] - k_{-6}[\text{AMD}] \approx k_6[\text{AM*D}] \quad (19)$$

From a study carried out by Sleep and Hutton (1980), K_6 is estimated to be 50–100, hence $k_6 \gg k_{-6}$. Furthermore, since [AM*D]≫[AMD] (this report), we can ignore the reversal term in Eq. 19 for all practical purposes. This enables us to calculate k_6 from the ATP hydrolysis rate in muscle fibers. Potma et al. (1995) reported that at 15°C and pH 7.3, the ATPase activity is ~8× lower in rabbit soleus than in rabbit psoas fibers. Our previous estimate is that k_6 in psoas is 9–16 s^{-1} (Kawai and Halvorson, 1991; Zhao and Kawai, 1993). In this report the probability of cross-bridges in the AM*D state is 20% in soleus STF and 32% in psoas. If we assume that the myosin concentration is not very different between these two fiber types, we can estimate k_6 in soleus STF. Our calculation shows that k_6 is ~1.5–3 s^{-1} in rabbit soleus STF. The fact that step 6 is the slowest step in the cross-bridge cycle in soleus STF is consistent with the result in rabbit psoas fibers (Kawai and Halvorson, 1991; Kawai and Zhao, 1993) and in ferret myocardium (Kawai et al., 1993).

Transient analyses (e.g., sinusoidal analysis/step analysis, pressure-release and caged-ligand experiments) are not sensitive to the slowest step in the cross-bridge cycle; hence, step 6 cannot be resolved in transient analyses, and process **A** could not be correlated with step 6. Earlier reports have demonstrated that force generation and oscillatory work production occur in the absence of process **A** in insect fibers (Machin and Pringle, 1960; Marcussen and Kawai, 1990), cardiac preparations, and in partially cross-linked rabbit psoas fibers (Tawada and Kawai, 1990). These experiments suggested that process **A** does not represent an elementary step in the cross-bridge cycle, but rather it corresponds to sarcomere instability (Tawada and Kawai, 1990). Thus, the

ATP hydrolysis rate measurement is a convenient method to characterize the rate-limiting step 6.

Because step 6 is the slowest step of all elementary steps, we can approximate the cross-bridge cycle by opening it at step 6, i.e., we can assume that step 6 does not occur for the purpose of analyzing the results of tension transients. This simplifies the analysis of an otherwise complex cycle, and enables an algebraic realization such as shown in Eqs. 3–5 that relate apparent rate constants to the kinetic constants of elementary steps in simple mathematical formulae. This method of approach is advantageous over the commonly used numerical analysis method (e.g., Iwamoto, 1995; Murase et al., 1986), because the experimental results can be readily correlated with the cross-bridge model.

Filament compliance and measured stiffness

Recent findings that thick and thin filaments are compliant as well as cross-bridges (Bagni et al., 1990; Wakabayashi et al., 1994; Huxley et al., 1994; Higuchi et al., 1995) in rabbit psoas fibers may need some consideration. Each of these elements may carry ~⅓ of the total compliance at full activation (Wakabayashi et al., 1994). If this is the case, then measured stiffness (Y_∞) is not proportionately related to the number of attached cross-bridges (n), but rather it is a concave function of n. According to one analysis (Mijailovich et al., 1996), however, the concavity is not very different from the proportionality, and qualitative features such as "higher Y_∞ indicates more attached cross-bridges" do not change. Similarly, the extra compliance may change the measured rate constant somewhat, but it does not change the equilibrium constants. This aspect was discussed in our previous paper (Wang and Kawai, 1996).

Number of attached cross-bridges during control activation

We examined the ratio Y_∞ to Y_{rig} during control activation. This ratio (63 ± 3%) represents the number of (strongly) attached cross-bridges during the control activation, which is calculated to be 78% based on Eqs. 13 and 14 and the kinetic constants in Table 2. Thus, there was considerable agreement between the predicted value and the value based on the stiffness measurement. The small disagreement (63% vs. 78%) may relate to the fact that thick and thin filaments are compliant as discussed above.

Rigor state

It is interesting to know if the AM state during the cross-bridge cycle is equivalent to the rigor state induced with a reduction of the MgATP concentration. For this purpose we compared tension and stiffness of both states. Since the rigor state is not uniquely defined and depends on the condition in which the fiber is placed before rigor induction, we used the high-rigor state (Kawai and Brandt, 1976) which was induced after the fiber was fully activated by the control activating solution A (Fig. 7). Tension and stiffness values are expressed with respect to T_c (control tension). Our findings show that T_{1a} (tension of the AM state) is 1.12 T_c, and this is in agreement with T_{rig} (1.08 ± 0.04 T_c), which is tension measured after rigor induction. Our results further demonstrate that Y_a (stiffness of the AM state) is 98 T_c and approximates Y_{rig} (118 ± 7 T_c), which is stiffness measured after rigor induction. Similar results were obtained with rabbit psoas fibers (Kawai and Zhao, 1993). From these results, we infer that the AM state that exists when the cross-bridges are fully active is the same cross-bridge state that is attained after induction of the high-rigor state.

Stiffness and the tension-to-stiffness ratio

Stiffness results (Fig. 6, *solid line*) fit satisfactorily to Eq. 18, indicating that all (strongly) attached cross-bridges contribute similarly to stiffness. Fig. 8 demonstrates that the tension/stiffness ratio decreased as the Pi concentration was increased, which implies that cross-bridge populations are shifted to the state(s) that supports less tension at higher Pi concentrations. This observation is consistent with Scheme 6, and the results fit well to Eqs. 16 and 18 (solid line, Figs. 6 and 8) that are based on Scheme 6. If the Pi concentration is increased, the equilibrium shifts to the left to result in an

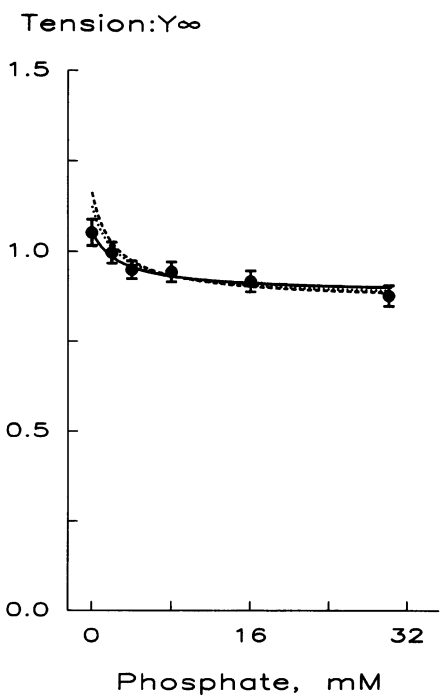

FIGURE 8 The tension to Y_∞ ratio is plotted against the Pi concentration. The $MgATP^{2-}$ concentration was 5 mM. The data were normalized to those from the initial control activation, then averaging was performed over nine experiments and plotted with mean ± SE bars. Theoretical projections (curved lines) are based on Eqs. 16 and 20. (—), q = 0 (no series compliance); (· · ·), q = 0.5 Y_c^{-1}; (- - -), q = 1.0 Y_c^{-1}.

increase in the AM*S state. This state has less tension than the AM*DP or AM*D state, but it has the same stiffness as others, thus accounting for the results shown in Fig. 8.

The second explanation of the extra stiffness at high Pi concentration may be that the strongly attached low-force state might exist before force generation (Cecchi et al., 1982; Martyn and Gordon, 1992; Regnier et al., 1995). The early evidence for the strongly attached low-force state is based on the observation that the stiffness time course is faster than the tension time course on electrical stimulation of intact frog fibers (Cecchi et al., 1982). However, this delay of tension rise can also be explained by the delay in stretching in-series elements to cross-bridges, such as thick and thin filaments, as suggested by Goldman and Huxley (1994). The second evidence is based on extra stiffness at high Pi concentrations (Martyn and Gordon, 1992; Regnier et al., 1995), similar to our Fig. 8. As discussed above, in our model this extra stiffness can be explained by the AM*S state, which has low tension. The existence of this state was not considered in models used by Martyn and Gordon (1992) or by Regnier et al. (1995).

The third explanation of the extra stiffness at high Pi concentration may be related to the filament compliance as discussed above. This situation is depicted in Fig. 9. In this figure, q indicates the filament compliance (series compliance), z indicates cross-bridge compliance, and n is the number of attached cross-bridges. The overall tension is proportional to n, and overall compliance is proportional to $q + z/n$. Thus, tension to stiffness ratio becomes proportional to $nq + z$, because stiffness is the reciprocal of compliance. This analysis indicates that the ratio becomes larger as the number of attached cross-bridges increases. This prediction appears to be consistent with the data shown in Fig. 8. In reality, both this mechanism and a shift in the population (first mechanism discussed above) would take place as the ligand (e.g., Pi) concentration is changed.

Thus, we further fitted the stiffness data to Eq. 20, which considers filament compliance q and is modified from Eq. 18:

$$1/Y_\infty = 1/Y_a X_{att} + q$$

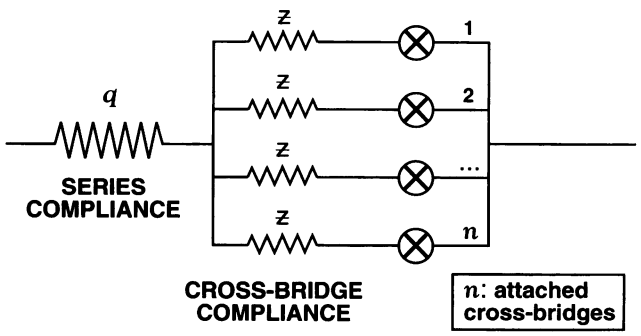

FIGURE 9 Schematic drawing of a model of activated muscle fiber. q stands for series compliance, z stands for cross-bridge compliance, and ⊗ stands for attached cross-bridges.

or

$$Y_\infty = \frac{Y_a X_{att}}{1 + Y_a X_{att} q} \quad (20)$$

Equations 15–17, which describe isometric tension, are not modified by the inclusion of series compliance. The results of fitting the stiffness data for $q = 0.5\ Y_c^{-1} = 0.64\ Y_a^{-1}$ is entered in Figs. 6 and 8 in dotted lines (· · ·), and for $q = 1.0\ Y_c^{-1} = 1.27\ Y_a^{-1}$ in broken lines (- - -). The solid lines (—) correspond to $q = 0$ (no series compliance). $q = 0.64\ Y_a^{-1}$ corresponds to 39% series compliance (61% cross-bridge compliance), and $q = 1.27\ Y_a^{-1}$ to 56% series compliance (44% cross-bridge compliance). In Fig. 6, the shape of the solid curves cannot be changed, because they come directly from Eq. 13 (X_{att}) and as shown in Fig. 3 (curves labeled **Att**). As Figs. 6 and 8 demonstrate, the data fitting becomes progressively worse as q is increased from 0 to $1.27\ Y_c^{-1}$. Therefore, it can be concluded that the effect of series compliance is small or negligible under our experimental conditions. In other words, a good fit of the stiffness results (Fig. 6, *solid line*) or the tension-to-stiffness ratio (Fig. 8, *solid line*) to Eqs. 16 and 18 implies that most of the Pi effect is explained by the population shift, and little room is left for the filament compliance.

CONCLUSIONS

We found that the elementary steps of the cross-bridge cycle are the same in soleus STF, psoas (FTF), and myocardium (Scheme 6), from which we conclude that the mechanism of force generation is similar in different muscle types. The rate constants of the elementary steps in soleus STF are ~20× smaller than those of psoas, and ~2× smaller than those of myocardium (Table 2). The phosphate association constant (K_5) of soleus STF is 1.5× that of psoas, and 3× that of myocardium, which explains the slightly higher Pi sensitivity in suppressing isometric tension in soleus STF than in FTF. As in psoas fibers, force generation occurs with the isomerization of the AM.ADP.Pi state (step 4) and before Pi release (step 5). In general, we found that cross-bridge force gradually decreases with sequential isomerizations (conformational changes) during which cross-bridges are attached to actin, and which follows/precedes the binding/release of ligands (ATP, ADP, Pi) (Table 3). Our results are consistent with the hypothesis that isomerization of the AM.ADP state (step 6) is the slowest step in the cross-bridge cycle. Our analysis indicates that the effect of filament compliance is almost negligible under our experimental conditions.

The authors thank Karen Humphries for carrying out the comparative experiments on rabbit psoas fibers.

This study was supported by the National Science Foundation (Grants IBN 93-18120 and IBN 96-03858) and the American Heart Association (Iowa affiliate, Grant IA-94-GS-45).

REFERENCES

Altringham, J. D., and I. A. Johnston. 1985. Effects of phosphate on the contraction properties of fast and slow muscle fibres from an antarctic fish. *J. Physiol. (Lond.).* 368:491–500.

Bagni, M. A., G. Cecchi, F. Colomo, and C. Poggesi. 1990. Tension and stiffness of frog muscle fibres at full filament overlap. *J. Muscle Res. Cell Motil.* 11:371–377.

Bagshaw, C. R., and D. R. Trentham. 1974. The characterization of myosin-product complexes and of product-release steps during the magnesium ion-dependent adenosine triphosphatase reaction. *Biochem. J.* 141:331–349.

Brenner, B., L. C. Yu, and J. M. Chalovich. 1991. Parallel inhibition of active force and relaxed fiber stiffness in skeletal muscle by caldesmon: implications for the pathway to force generation. *Proc. Natl. Acad. Sci. U.S.A.* 88:5739–5743.

Cecchi, G., P. J. Griffiths, and S. Taylor. 1982. Muscular contraction: kinetics of cross-bridge attachment studied by high-frequency stiffness measurements. *Science.* 217:70–72.

Dantzig, J., Y. Goldman, N. C. Millar, J. Lacktis, and E. Homsher. 1992. Reversal of the cross-bridge force-generating transition by the photogeneration of phosphate in rabbit psoas muscle fibers. *J. Physiol. (Lond.).* 451:247–278.

Ford. L. E., A. F. Huxley, and R. M. Simmons. 1977. Tension responses to sudden length change in stimulated frog muscle fibres near slack length. *J. Physiol.* 269:441–515.

Fortune, N. S., M. A. Geeves, and K. W. Ranatunga. 1991. Tension responses to rapid pressure release in glycerinated rabbit muscle fibers. *Proc. Natl. Acad. Sci. U.S.A.* 88:7323–7327.

Fryer, M. W., V. J. Owen, G. D. Lamb, and D. G. Stephenson. 1995. Effects of creatine phosphate and Pi on Ca^{2+} movements and tension development in rat skinned skeletal muscle fibers. *J. Physiol.* 482.1: 123–140.

Galler, S., T. L. Schmitt, and D. Pette. 1994. Stretch activation, unloaded shortening velocity, and myosin heavy chain isoforms of rat skeletal muscle fibers. *J. Physiol. (Lond.).* 478.3:513–521.

Gillis, J. M., and G. Maréchal. 1974. The incorporation of radioactive phosphate into ATP in glycerinated fibers stretched or released during contraction. *J. Mechanochem. Cell Motil.* 3:55–68.

Godt, R. E., and D. W. Maughan. 1988. On the composition of the cytosol of relaxed skeletal muscle of the frog. *Am. J. Physiol.* 254:C591–C604.

Godt, R. E., and T. M. Nosek. 1989. Changes of intracellular milieu with fatigue or hypoxia depress contraction of skinned rabbit skeletal and cardiac muscle. *J. Physiol. (Lond.).* 412:155–180.

Goldman, Y. E., and A. F. Huxley. 1994. Actin compliance: are you pulling my chain? *Biophys. J.* 67:2131–2133.

Hammes, G. G. 1968. Relaxation spectrometry of biological systems. *Adv. Protein. Chem.* 23:1–57.

Heinl, P., H. J. Kuhn, and J. C. Rüegg. 1974. Tension responses to quick length changes of glycerinated skeletal muscle fibres from the frog and tortoise. *J. Physiol. (Lond.).* 237:243–258.

Herzig, J. W., J. W. Peterson, R. J. Solaro, and J. C. Rüegg. 1982. Phosphate and vanadate reduce the efficiency of the chemomechanical energy transformation in cardiac muscle. *In* Regulation of Phosphate and Mineral Metabolism. S. G. Massry, J. M. Letteri, and E. Ritz, editors. Plenum Publishing Corp., New York. 267–281.

Herzig, J. W., and J. C. Rüegg. 1977. Myocardial cross-bridge activity and its regulation by Ca^{2+}, phosphate, and stretch. *In* Myocardial Failure. G. Rieker, A. Weber, and J. Goodwin, editors. Springer-Verlag, New York. 41–51.

Hibberd, M. G., M. R. Webb, Y. Goldman, and D. R. Trentham. 1985. Oxygen exchange between phosphate and water accompanies calcium-regulated ATPase activity of skinned fibers from rabbit skeletal muscle. *J. Biol. Chem.* 260:3496–3500.

Higuchi, H., T. Yanagida, and Y. E. Goldman. 1995. Compliance of thin filaments in skinned fibers of rabbit skeletal muscle. *Biophys. J.* 69: 1000–1010.

Huxley, A. F., and R. M. Simmons. 1971. Proposed mechanism of force generation in striated muscle. *Nature (Lond.).* 233:533–538.

Huxley, H. E., A. Stewart, H. Sosa, and T. Irving. 1994. X-ray diffraction measurements of the extensibility of actin and myosin filaments in contracting muscle. *Biophys. J.* 67:2411–2421.

Iwamoto, H. 1995. Simple modelling of linear and nonlinear mechanical responses to sinusoidal oscillations during muscle contraction. *J. Muscle Res. Cell Motil.* 16:249–256.

Kawai, M. 1986. The role of orthophosphate in crossbridge kinetics in chemically skinned rabbit psoas fibres as detected with sinusoidal and step length alterations. *J. Muscle Res. Cell Motil.* 7:421–434.

Kawai, M., and P. W. Brandt. 1976. Two rigor states in skinned crayfish single muscle fibers. *J. Gen. Physiol.* 68:267–280.

Kawai, M., and P. W. Brandt. 1980. Sinusoidal analysis: a high resolution method for correlating biochemical reactions with physiological processes in activated skeletal muscles of rabbit, frog and crayfish. *J. Muscle Res. Cell Motil.* 1:279–303.

Kawai, M., and H. R. Halvorson. 1991. Two step mechanism of phosphate release and the mechanism of force generation in chemically skinned fibers of rabbit psoas muscle. *Biophys. J.* 59:329–342.

Kawai, M., Y. Saeki, and Y. Zhao. 1993. Cross-bridge scheme and kinetic constants of elementary steps deduced from chemically skinned papillary and trabecular muscles of the ferret. *Circ. Res.* 73:35–50.

Kawai, M., and F. H. Schachat. 1984. Differences in the transient response of fast and slow skeletal muscle fibers: correlations between complex modulus and myosin light chain. *Biophys. J.* 45:1145–1151.

Kawai, M., and Y. Zhao. 1993. Cross-bridge scheme and force per cross-bridge state in skinned rabbit psoas muscle fibers. *Biophys. J.* 65: 638–651.

Kentish, J. C. 1986. The effects of inorganic phosphate and creatine phosphate on force production in skinned muscles from rat ventricle. *J. Physiol.* 370:585–604.

Kentish, J. C. 1991. Combined inhibitory acidosis and phosphate on maximum force production in rat skinned cardiac muscle. *Pfluegers Arch.* 419:310–318.

Machin, K. E., and J. W. S. Pringle. 1960. The physiology of insect fibrillar muscle. III. The effect of sinusoidal changes of length on a beetle flight muscle. *Proc. Roy. Soc. B.* 152:311–330.

Mannherz, H. G. 1970. On the reversibility of the biochemical reactions of muscular contraction during the absorption of negative work. *FEBS Lett.* 10:233–236.

Marcussen, B. L., and M. Kawai. 1990. Role of MgATP and inorganic phosphate ions in cross-bridge kinetics in insect (*Lethocerus colossicus*) flight muscle. *In* Frontiers in Smooth Muscle Research. Alan R. Liss, Inc. 805–813.

Martyn, D. A., and A. M. Gordon. 1992. Force and stiffness in glycerinated rabbit psoas fibers. *J. Gen. Physiol.* 99:795–816.

Meyer, R. A., T. R. Brown, and M. J. Kushmerick. 1985. Phosphorus nuclear magnetic resonance of fast- and slow-twitch muscle. *Am. J. Physiol.* 248:C279–C287.

Mijailovich, S. M., J. J. Fredberg, and J. P. Butler. 1996. On the theory of muscle contraction: filament extensibility and the development of isometric force and stiffness. *Biophys. J.* 71:1475–1484.

Millar, N. C., and E. Homsher. 1990. The effect of phosphate and calcium on force generation in glycerinated rabbit skeletal muscle fibers. *J. Biol. Chem.* 265:20234–20240.

Millar, N. C., and E. Homsher. 1992. Kinetics of force generation and phosphate release in skinned rabbit soleus muscle fibers. *Am. J. Physiol.* 252:C1239–C1245.

Murase, M., H. Tanaka, K. Nishiyama, and H. Shimizu. 1986. A three-state model for oscillation in muscle: sinusoidal analysis. *J. Muscle Res. Cell Motil.* 7:2–10.

Nosek, T. M., K. Y. Fender, and R. E. Godt. 1987. It is diprotonated inorganic phosphate that depresses force in skinned skeletal muscle fibers. *Science.* 236:191–193.

Nosek, T. M., J. H. Leal-Cardoso, M. McLaughlin, and R. E. Godt. 1990. Inhibitory influence of phosphate and arsenate on contraction of skinned skeletal and cardiac muscle. *Am. J. Physiol.* 259:C933–C939.

Pate, E., and R. Cooke. 1989. Addition of phosphate to active muscle fibers probes actomyosin states within the power stroke. *Pfluegers Arch.* 414:73–81.

Potma, E. J., I. A. van Graas, and G. J. M. Stienen. 1995. Influence of Inorganic phosphate and pH on ATP utilization in fast and slow skeletal muscle fibers. *Biophys. J.* 69:2580–2589.

Regnier, M., C. Morris, and E. Homsher. 1995. Regulation of the cross-bridge transition from a weakly to strongly bound state in skinned rabbit muscle fibers. *Am. J. Physiol.* 269:C1532–C1539.

Rüegg, J. C., M. Schädler, G. J. Steiger, and G. Muller. 1971. Effects of inorganic phosphate on the contractile mechanism. *Pfluegers Arch.* 325:359–364.

Schoenberg, M. 1988. Characterization of the myosin adenosine triphosphate (M. ATP) crossbridge in rabbit and frog skeletal muscle fibers. *Biophys. J.* 54:135–148.

Sleep, J. A., and R. L. Hutton. 1980. Exchange between inorganic phosphate and adenosine 5′-triphosphate in the medium by actomyosin subfragment 1. *Biochemistry.* 19:1276–1283.

Stein, L. A., R. P. Schwartz, Jr., P. B. Chock, and E. Eisenberg. 1979. Mechanism of actomyosin adenosine triphosphatase. Evidence that adenosine 5′-triphosphate hydrolysis can occur without dissociation of the actomyosin complex. *Biochemistry.* 18:3895–3909.

Stienen, G. J. M., P. G. A. Versteeg, Z. Papp, and E. Elzinga. 1992. Mechanical properties of skinned psoas and soleus muscle fibers during lengthening: effects of phosphate and Ca^{2+}. *J. Physiol. (Lond.).* 451: 503–523.

Tawada, K., and M. Kawai. 1990. Covalent cross-linking of single muscle fibers from rabbit psoas increases oscillatory power. *Biophys. J.* 57: 643–647.

Taylor, E. W. 1979. Mechanism of actomyosin ATPase and the problem of muscle contraction. *CRC Crit. Rev. Biochem.* 6:103–164.

Ulbrich, M., and J. C. Rüegg. 1971. Stretch induced formation of ATP-^{32}P in glycerinated fibres of insect flight muscle. *Experientia.* 27:45–46.

Wakabayashi, K., Y. Sugimoto, H. Tanaka, Y. Ueno, Y. Takezawa, and Y. Amemiya. 1994. X-ray diffraction evidence for the extensibility of actin and myosin filaments during muscle contraction. *Biophys. J.* 67: 2422–2435.

Walker, J. W., Z. Lu, and R. L. Moss. 1992. Effects of Ca^{2+} on the kinetics of phosphate release in skeletal muscle. *J. Biol. Chem.* 267:2459–2466.

Wang, G., and M. Kawai. 1995. Temperature effect on elementary steps of the cross-bridge cycle in rabbit soleus muscle fibers. *Biophys. J.* 68:A17 (Abstr.).

Wang, G., and M. Kawai. 1996. Effects of MgATP and MgADP on the cross-bridge kinetics of rabbit soleus slow-twitch muscle fibers. *Biophys. J.* 71:1450–1461.

Wang, G., Y. Zhao, and M. Kawai. 1994. Elementary steps of the cross-bridge cycle in rabbit soleus muscle fibers. *Biophys. J.* 66:A304 (Abstr.).

White, H. D., and E. W. Taylor. 1976. Energetics and mechanism of actomyosin adenosine triphosphate. *Biochemistry.* 15:5818–5826.

White, D. C. S., and J. T. Thorson. 1972. Phosphate starvation and the nonlinear dynamics of insect fibrillar flight muscle. *J. Gen. Physiol.* 60:307–336.

Zhao, Y., and M. Kawai. 1993. The effect of the lattice spacing on cross-bridge kinetics in chemically skinned psoas fibers. II. Elementary steps affected by the spacing change. *Biophys. J.* 64:197–210.